Available online at www.sciencedirect.com
ScienceDirect
International Journal of Heat and Mass Transfer 50 (2007) 444–451
International Journal of HEAT and MASS TRANSFER
www.elsevier.com/locate/ijhmt

Effect of curvature ratios on the heat transfer and flow developments in the horizontal spirally coiled tubes

Paisarn Naphon *, Jamnean Suwagrai

Department of Mechanical Engineering, Faculty of Engineering, Srinakharinwirot University, 63 Rangsit-Nakhonnayok Road, Ongkharak, Nakhon-Nayok 26120, Thailand

Received 18 December 2005; received in revised form 2 August 2006
Available online 19 October 2006

Abstract

Effect of curvature ratios on the heat transfer and flow developments in the horizontal spirally coiled tubes are investigated. The spirally coiled tube is fabricated by bending a 8.00 mm diameter straight copper tube into a spiral-coil of five turns. The spirally coiled tube with three different curvature ratios of 0.02, 0.04, 0.05 under constant wall temperature are tested. Cold water entering the innermost turn flows along the spiral tube and flows out at the outermost turn. The turbulent flow and heat transfer developments are simulated by using the k–ε standard turbulence model. A finite volume method with an unstructured nonuniform grid system is employed for solving the model. The simulated results are validated by comparing with the present experiment. The predicted results for the convective heat transfer and flow characteristics are reasonable agreement with the experiments. The centrifugal force has significant effect on the enhancements of heat transfer and pressure drop. In addition, due to this force, the heat transfer and pressure drop obtained from the spirally coiled tube are higher than those from the straight tube.

Keywords: Heat transfer development; Flow development; Spirally coiled tube; Curvature ratio

1. Introduction

Turbulent flow and convective heat transfer in a spirally coiled tube are complicated as comparing the straight tube. This is because the heat transfer and flow developments in the curved tube strongly depend on the behavior of secondary flow. The secondary flow in the curved tube is caused by the centrifugal force. Helical and spiral coils are well known types of curved tubes which have been used in a wide variety of applications. However, most studies for curved tubes are concerned with the helically coiled heat exchanger [1]. Prabhanjan et al. [2] experimentally studied on the natural convection heat transfer from helical coiled tubes in water. The predicted outlet temperature was compared with the measured values from an experimental setup. Palazoglua and Sandeep [3] considered effect of tube curvature ratio on the residence time distribution of multiple particles in helical tubes. All of the parameters, except the carrier fluid viscosity, had strong effects on the flow behavior of particles. Ceresa et al. [4] collected the atmospheric moisture from a continuous air flow through a refrigerated coil tube. Ko and Ting [5,6] studied entropy generation, thermodynamics and Reynolds number optimizations of fully developed laminar convection in a helical coil with constant heat flux. In their third and fourth papers, Ko and Ting [7,8] analyzed the optimal mass flow rate and curvature ratio for fully developed laminar forced convection in a helical coiled tube with constant heat flux based on minimal entropy generation principle. Air and water were used as working fluids. Murai et al. [9] experimentally investigated effects of centrifugal acceleration on the flow regime map and the spatial and the temporal flow structure distribution of air–water two-phase flow in helically coiled tubes. Cioncolini and Santini [10] carried out

* Corresponding author. Tel.: +6637 322625x2065; fax: +6637 322609.
E-mail address: paisarnn@swu.ac.th (P. Naphon).

0017-9310/$ - see front matter © 2006 Elsevier Ltd. All rights reserved.
doi:10.1016/j.ijheatmasstransfer.2006.08.002

Nomenclature

A	surface area, m^2
$C_{\varepsilon 2}$	turbulent model constant
c_p	specific heat, kJ/kg °C
d_i	tube diameter, m
H	length of tube, m
k	turbulent kinetic energy, m^2/s^2
m_w	water mass flow rate, kg/s
p	pressure, kN/m^2
Q	heat transfer rate (kW)
r	radius coordinate
T	temperature, °C
u	velocity in axial direction, m/s
w	velocity in azimuthal direction, m/s
$C_{\varepsilon 1}$	turbulent model constant
C_μ	turbulent model constant
C_R	curvature ratio
f	friction factor
I	turbulent intensity
L	turbulence characteristics length, m
Nu	Nusselt number
Pr	Prandtl number
R	residual parameter
Re	Reynolds number
t	time, s
v	velocity in radius direction, m/s
z	axial coordinate, m

Greek symbols

ϕ	azimuthal coordinate
ρ	density, kg/m^3
Φ	viscosity energy dissipation function
σ_ε	diffusion Prandtl number for ε
ε	dissipation kinetic energy, m^2/s^3
μ	viscosity, kg/ms
σ_k	diffusion Prandtl number for k
τ	shear stress

Subscripts

ave	average
c	curve
l	laminar
χ	parameter
tu	tube
w	water
b	bulk
in	inlet
max	maximum
t	turbulent
wall	wall

to investigate the transition from laminar to turbulent flow in helically coiled pipes. Twelve coils have different ratios of coil diameter to tube diameter were tested. Kumar et al. [11] studied the mixing efficiency in a curved tube. In this work, a computational fluid dynamics study was performed in curved tubes of circular cross-section of finite pitch under laminar flow conditions to examine the scalar mixing of two miscible fluids using scalar transport technique.

Compared to the numerous investigations in the helically coiled tubes, there are few researchers on the heat transfer in the spiral-coil heat exchangers as in open literature [1]. Ho et al. [12,13] used the relevant correlations of the tube-side and air-side heat transfer coefficients in the simulation to determine the thermal performance of the spiral-coil heat exchanger under cooling and dehumidifying conditions. Nakayama et al. [14] numerically studied the cooling a fluid flowing through a spiral coil immersed in a chilled water container. A simple axisymmetric numerical procedure was described to determine the temperature of the fluid in the spiral coil and that of the coil surface. Naphon and Wongwises [15,16] modified the mathematical model of Ho et al. [13] by including the fin efficiency and using the other existing the heat transfer coefficient correlations to determine the performance and heat transfer characteristics of spiral-coil tube heat exchanger under wet-surface conditions. The relevant parameters on the performance of the heat exchanger were discussed.

Due to the complex study on heat transfer and flow developments in each layer of the spirally coiled tube of the spiral-coil heat exchanger, investigation on the heat transfer in spiral-coil heat exchangers has received comparatively little attention in literature, especially numerical study. The objective of this paper is to study the heat transfer and flow characteristics in the horizontal spirally coiled tube of the spiral-coil heat exchanger. Effects of curvature ratios and relevant parameters on the heat transfer and flow characteristics are discussed. Numerical results are verified by comparing with the present measured data.

2. Experimental apparatus and procedure

Fig. 1 shows a schematic diagram of the experimental apparatus. The experimental set up is composed of a test section, refrigerant loop, cold water loop and data acquisition system. The test section and the connections of the piping system are designed such that parts can be changed or repaired easily. The test section is the horizontal spirally coiled tube which immerged inside the hot water storage tank. The close-loop of cold water consists of a 0.5 m^3 storage tank, an electric heater controlled by adjusting the voltage, and a cooling coil immerged inside a storage tank. The

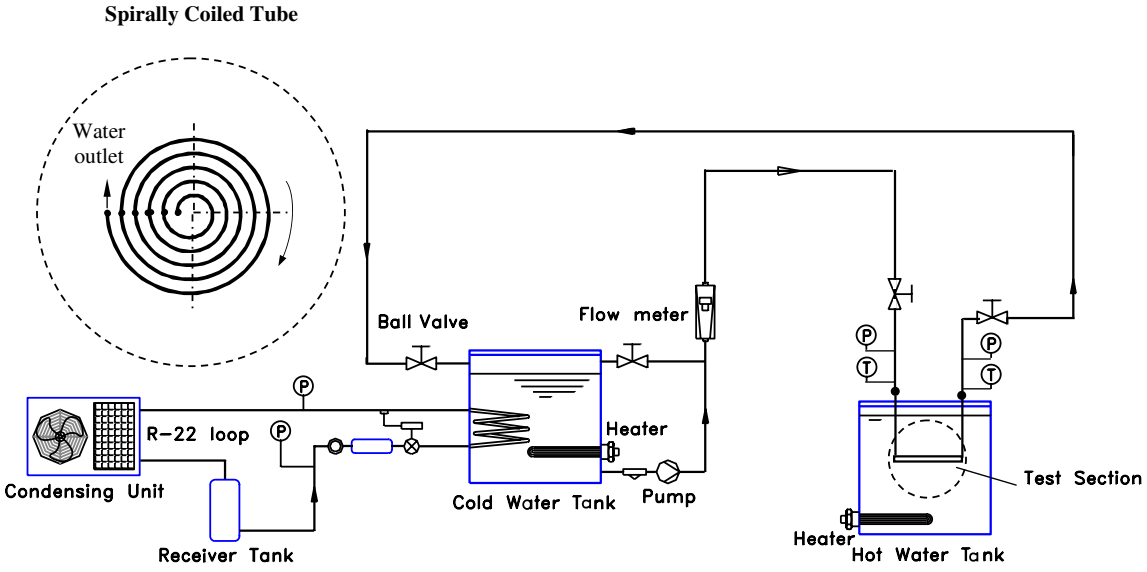

Fig. 1. Schematic diagram of experimental apparatus.

cold water is chilled by the refrigeration system. The hot and cold water are adjusted to the desired level and controlled by temperature controller. After the temperature of the cold water is adjusted to achieve the desired level, the cold water is pumped out of the storage tank, and is passed through a flow meter, test section, and returned to the cold water storage tank. The flow rate of the cold water is controlled by adjusting the valve and measured by the flow meter with the accuracy of ±0.2% of full scale. The test section is fabricated from the straight copper tube. The dimensions of the test section are listed in Table 1.

Table 1
Dimensions of the horizontal spirally coiled tubes

Parameters	Dimensions
Outer diameter of tube, mm	9.60
Inner diameter of tube, mm	8.00
Length of test section, mm	5200, 4800, 4000
Pitches of spirally coiled tube, mm	30, 20, 18
Curvature ratio, (r_t/r_c)	0.02, 0.04, 0.05
Number of coil turns	5

The water temperature is measured in six positions with type T copper-constantan thermocouples by extending inside the tube as shown in Fig. 2. The accuracy of the type T copper-constantan thermocouple is ±0.10% of full scale. In addition, all the thermocouples are precalibrated by

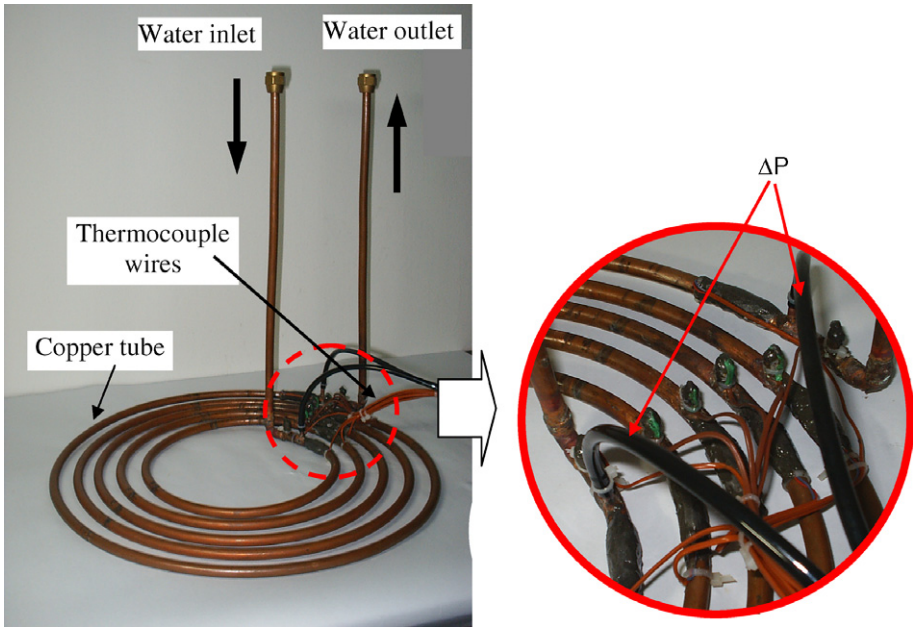

Fig. 2. Photograph of the horizontal spirally coiled tube used in the present study.

Table 2
Experimental conditions

Variables	Range
Inlet-cold water temperature, °C	20–25
Inlet-hot water temperature, °C	45–60
Cold water mass flow rate, kg/s	0.02–0.16

Table 3
Accuracy and uncertainty of measurements

Instruments	Accuracy	Uncertainty
Rotameter (kg/s)	0.2%	±0.10
Thermocouple type T, Data logger (°C)	0.1%	±0.10
Differential pressure transducer	0.02%	±0.02

dry-box temperature calibrator. The differential pressure transducer with the accuracy of ±0.02% of full scale is employed to measure the pressure drop.

Experiments were conducted with various temperatures of hot and cold water, and flow rate of cold water entering the test section. In the experiments, the cold water flow rate was increased in small increments while cold water and hot water temperatures were kept constant. The hot and cold water temperatures were adjusted to achieve the desired level by using electric heaters controlled by temperature controllers. Before any data were recorded, the system was allowed to approach the steady state. Data collection was carried out using a data acquisition system which all data were recorded three times. Temperatures at each position and pressure drops were averaged over the time period. The range of experimental conditions in this study, uncertainty and accuracy of the measurement are given in Tables 2 and 3, respectively.

3. Mathematical modelling

By considering the geometry and physical problem as shown in Fig. 3, the k–ε standard turbulence model [17] is used to simulate the turbulent flow and heat transfer developments. The fully elliptic differential governing equations of the unsteady turbulent flow in the spirally coiled tube can be written in the following forms:
Continuity equation:

$$\frac{\partial u}{\partial z}+\frac{1}{r}\frac{\partial}{\partial r}(vr)+\frac{1}{r}\frac{\partial w}{\partial \phi}=0 \tag{1}$$

Momentum equation:
For r axis

$$\frac{Dv}{Dt}-\frac{w^2}{r}=-\frac{1}{\rho}\frac{\partial p}{\partial r}+\frac{\mu}{\rho}\left[\nabla^2 v-\frac{v}{r^2}-\frac{2}{r^2}\frac{\partial w}{\partial \phi}\right] \tag{2}$$

For ϕ axis

$$\frac{Dw}{Dt}-\frac{vw}{r}=-\frac{1}{\rho r}\frac{\partial p}{\partial \phi}+\frac{\mu}{\rho}\left[\nabla^2 w+\frac{2}{r^2}\frac{\partial v}{\partial \phi}-\frac{w}{r^2}\right] \tag{3}$$

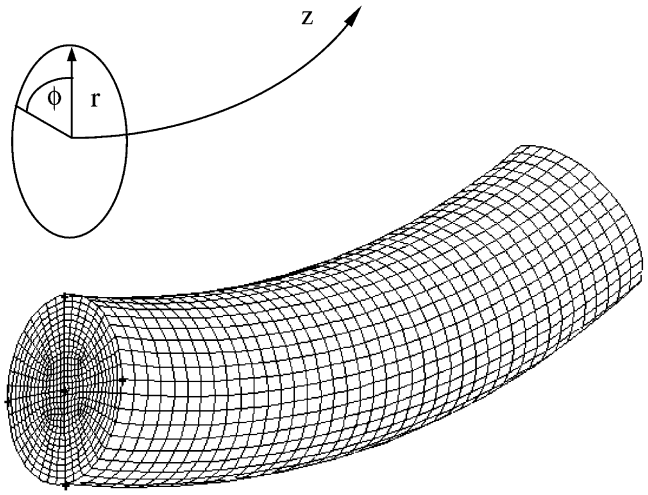

Fig. 3. Schematic diagram of the unstructured nonuniform grid system for spirally coiled tube.

For z axis

$$\frac{Du}{Dt}=-\frac{1}{\rho}\frac{\partial p}{\partial z}+\frac{\mu}{\rho}\nabla^2 u \tag{4}$$

Energy equation:

$$u\frac{\partial T}{\partial z}+v\frac{\partial T}{\partial r}+\frac{w}{r}\frac{\partial T}{\partial \phi}=\left(\frac{k}{\rho c_p}\right)\left[\frac{\partial^2 T}{\partial z^2}+\frac{1}{r}\frac{\partial}{\partial r}\left(r\frac{\partial T}{\partial r}\right)+\frac{1}{r^2}\frac{\partial^2 T}{\partial \phi^2}\right]+\left(\frac{\mu}{\rho c_p}\right)\Phi \tag{5}$$

where

$$\Phi=2\left[\left(\frac{\partial u}{\partial z}\right)^2+2\left(\frac{\partial v}{\partial r}\right)^2+\left(\frac{1}{r}\frac{\partial w}{\partial \phi}+\frac{v}{r}\right)^2\right]+\left[\frac{1}{r}\frac{\partial u}{\partial \phi}+\frac{\partial w}{\partial z}\right]^2+\left[\frac{\partial v}{\partial z}+\frac{\partial u}{\partial r}\right]^2+\left[\frac{1}{r}\frac{\partial v}{\partial \phi}+\frac{\partial w}{\partial r}-\frac{w}{r}\right]^2 \tag{6}$$

Turbulent kinetic energy (k) equation:

$$\frac{Dk}{Dt}=\frac{1}{\rho}\frac{\partial}{\partial y}\left[\left(\frac{\mu_t}{\sigma_k}+\mu_l\right)\frac{\partial k}{\partial y}\right]+\frac{\mu_t}{\rho}\left(\frac{\partial u}{\partial y}+\frac{\partial v}{\partial x}\right)\frac{\partial u}{\partial y}-\varepsilon \tag{7}$$

Turbulent kinetic energy dissipation (ε) equation:

$$\frac{D\varepsilon}{Dt}=\frac{1}{\rho}\frac{\partial}{\partial y}\left[\left(\frac{\mu_t}{\sigma_\varepsilon}+\mu_l\right)\frac{\partial \varepsilon}{\partial y}\right]+\frac{C_{\varepsilon 1}\mu_t}{\rho}\frac{\varepsilon}{k}\left(\frac{\partial u}{\partial y}+\frac{\partial v}{\partial x}\right)\frac{\partial u}{\partial y}-C_{\varepsilon 2}\frac{\varepsilon^2}{k} \tag{8}$$

The turbulent kinetic energy, k, and turbulent kinetic energy dissipation, ε, are coupled to the main governing equations via the turbulent viscosity relation ($\mu_t=\rho C_\mu k^2/\varepsilon$). The empirical constants for the turbulence model are arrived by comprehensive data fitting for a wide range of turbulent flow of Launder and Spalding [18]:

$$C_\mu = 0.09, \quad C_{\varepsilon 1} = 1.47, \quad C_{\varepsilon 2} = 1.92, \quad \sigma_k = 1.0, \quad \sigma_\varepsilon = 1.3 \tag{9}$$

Boundary conditions:

In the present study, noslip and isothermal boundary conditions are applied on the spirally coiled tube wall as follows:

$$u = 0, \quad v = 0, \quad w = 0, \quad T = T_{\text{wall}} \tag{10}$$

where u, v, w are the axial, radius and azimuthal velocities, respectively.

Initial conditions:

At the inlet boundary condition, the uniform profiles for all the properties are as follows:

$$u = u_{\text{in}}, \quad v = 0, \quad w = 0, \quad T = T_{\text{in}}, \quad k = k_{\text{in}}, \quad \varepsilon = \varepsilon_{\text{in}} \tag{11}$$

The turbulent kinetic energy, k_{in}, and the turbulent kinetic energy dissipation, ε_{in}, at the inlet section are approximated from the turbulent intensity, I, and a turbulent characteristics length, L, as follows:

$$k_{\text{in}} = \frac{3}{2}(u_{\text{in}} I)^2, \quad \varepsilon_{\text{in}} = C_\mu^{3/4} \frac{k^{3/2}}{L} \tag{12}$$

In the present study, the turbulence characteristics length, L, is set to be $0.07 r_{\text{tu}}$. The factor of 0.07 is based on the maximum value of the mixing length in the fully developed turbulent flow [19]. The turbulent intensity level, I, is defined the ratio of the root-mean-square of the velocity fluctuation, u', to the mean flow velocity, u, as follows:

$$I = \frac{u'}{u} \times 100\% \tag{13}$$

To represent the results and characterize the turbulent heat transfer and flow in the spirally coiled tube, the following variables and parameters are presented.

$$T_{\text{b,w}} = \frac{\int_0^A u_{\text{s}} T_{\text{w}} \mathrm{d}A}{\int_0^A u_{\text{s}} \mathrm{d}A} \tag{14}$$

$$Q_{\text{ave}} = m_{\text{w}} c_p (T_{\text{b,w,out}} - T_{\text{w,in}}) \tag{15}$$

$$Nu_\phi = \frac{(Q_{\text{ave}}/A_{\text{i}}) \cdot d_{\text{i}}}{\kappa (T_{\text{wall}} - T_{\text{b}})}, \quad Nu_{\text{ave}} = \frac{1}{2\pi} \int_0^{2\pi} Nu_\phi \mathrm{d}\phi \tag{16}$$

$$f_\phi = \frac{2\tau_\phi}{\rho u_{\text{in}}^2}, \quad f_{\text{ave}} = \frac{1}{2\pi} \int_0^{2\pi} f_\phi \mathrm{d}\phi \tag{17}$$

$$\frac{\Delta P_{\text{ave}}}{H} = \frac{f_{\text{ave}} \cdot \rho \cdot u_{\text{in}}^2}{2 \cdot d_{\text{i}}} \tag{18}$$

where τ_θ is local shear stress calculated with the normal velocity gradient at the wall, A_{i} is the inner tube surface area, κ is the thermal conductivity, u_{s} is the axial velocity, H is the length of the spirally coiled tube, and Q_{ave} is determined from the heat removal capacity by cold water.

4. Numerical computation

The governing equations (1)–(18), are a set of convection equations with velocity and pressure coupling. Based on the control volume method, SIMPLEC algorithm of Van Doormal and Raithby [20] is employed to deal with the problem of velocity and pressure coupling. Second-order upwind scheme and unstructured nonuniform grid system with 5.4×10^5 grids are used to discretize the main governing equations as shown in Fig. 3. A grid independence is carried out in the analysis by adopting different grid distributions of 4.0×10^5, 4.5×10^5, 5.4×10^5 and 6.5×10^5. The grid independence test indicated that the grid system of 5.4×10^5 ensure a satisfactory solution. This is verified by the fact that the difference of the computed results of temperature, friction factor, and heat transfer rate with grid finer than the 5.4×10^5 (e.g. 6.5×10^5) and those with the 5.4×10^5 grid within only 1%. At the inlet, fluid with turbulence intensity, I, and temperature, T_{in}, enters the spirally coiled tube at the velocity of u_{in}. The spirally coiled tube wall temperature is assumed to be an uniform tube wall temperature, $T_{\text{wall,ave}}$. Velocity boundary condition is applied at the inlet section while the pressure boundary condition is used at the outlet section. The commercial program FLUENT has been used as the numerical solver. The numerical computation is ended if the residual summed over all the computational nodes satisfies the following criterion:

$$\frac{R_\chi^n}{R_{\chi,\max}^m} \leqslant 10^{-5} \tag{19}$$

where R_χ^n is the residual at the nth iteration for variable, χ $(u, v, w, k, \varepsilon)$, and $R_{\chi,\max}^m$ is the maximum residual value after m iterations.

5. Results and discussion

Because there is almost no data as in the open literature on the heat transfer and flow characteristics in the spirally coiled tube, the predicted results are compared with the present experimental data. Fig. 4 shows the variation of the water temperatures with the position along the spiral tube for different cold water mass flow rates. The 1st and 6th positions are represented as the inlet and outlet sections of the horizontal spiral coil, respectively. The cold water entering the innermost turn flows along the spiral tube and flows out at the outermost turn. The test section is the spirally coiled tube which immerged inside the hot water tank. The experiments are carried out under constant tube wall temperature, for curvature ratios, $(r_{\text{tu}}/r_{\text{c}}) = 0.04$, 0.05, inlet cold water temperatures and average tube wall temperature of 25 and 35 °C, respectively.

As expected, the water temperature increases with increasing distance from the inlet section. However, at higher distance from the inlet section, this effect tends to decrease. It should be noted that when the cold water mass

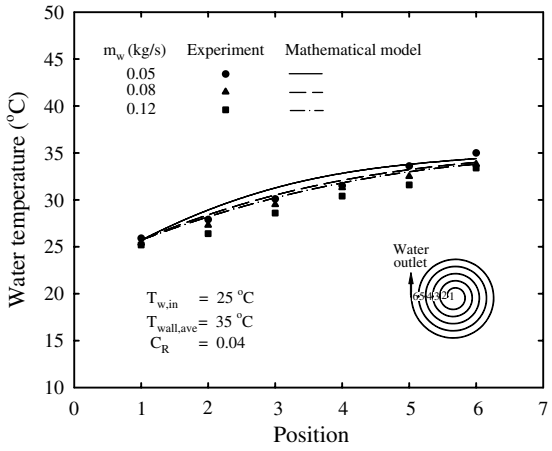

Fig. 4. Variation of water temperature with position of spirally coiled tube.

flow rate, the inlet cold water and average tube wall temperatures are kept constant, the water temperature at various positions decrease as the cold water mass flow rates increase. The average difference between the measured data is 7.50%. Fig. 4 also compares the results obtained from the present experiment and those from the numerical study. It can be clearly seen from figure that the results obtained from the model slightly overpredict the measured data.

Fig. 5 illustrates the variation of the outlet water temperature with water mass flow rate for different curvature ratios. It is found that when the inlet cold water and average tube wall temperatures are kept constant, the outlet water temperature decreases with increasing cold water mass flow rate. This is because the heat transfer rate increases as water mass flow rate increases. But, the increasing of the heat transfer is less than that of cold water mass flow rate. Therefore, the outlet water temperature tends to decrease as cold water mass flow rate increases. For a given water mass flow rate, the outlet water temperature at lower curvature ratio are higher than those at higher ones. This is because the tube length for lower curvature ratio is higher than that higher ones. Considering the results obtained from the numerical study and those from the measured data, it can be clearly seen that the predicted outlet water temperature is slightly higher than the measured one.

Figs. 6 and 7 show the variation of the heat transfer rate with cold water mass flow rate. As expected, the heat transfer rate is directly proportional to the water mass flow rate. In addition, it can be noted that the curvature ratios have significant effect on the heat transfer rate. The same explanation described above as for Figs. 6 and 7 can be given. However, this effect can be clearly seen at higher water mass flow rate. These figures also show the comparison between the predicted results and the measured data. It can be clearly seen that the results obtained from the experiment are very well agreement with those from the simulation study.

Figs. 8 and 9 show the variation of the average Nusselt number calculated from the present experiment with water mass flow rate at various curvature ratios. As expected, the average Nusselt number increases with increasing cold

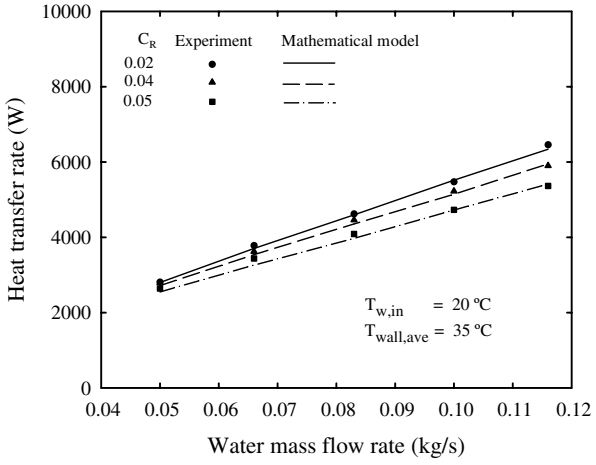

Fig. 6. Variation of heat transfer rate with water mass flow rate.

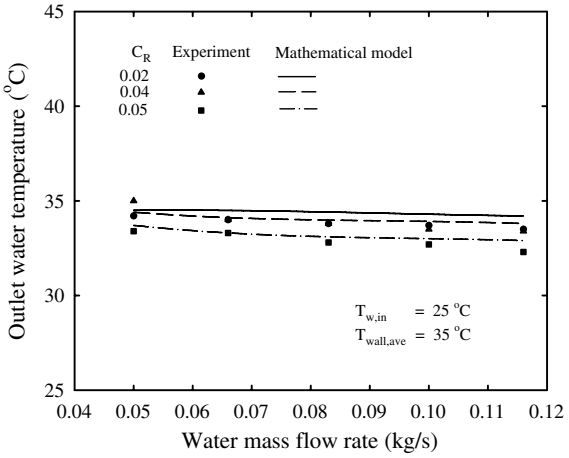

Fig. 5. Variation of outlet water temperature with water mass flow rate.

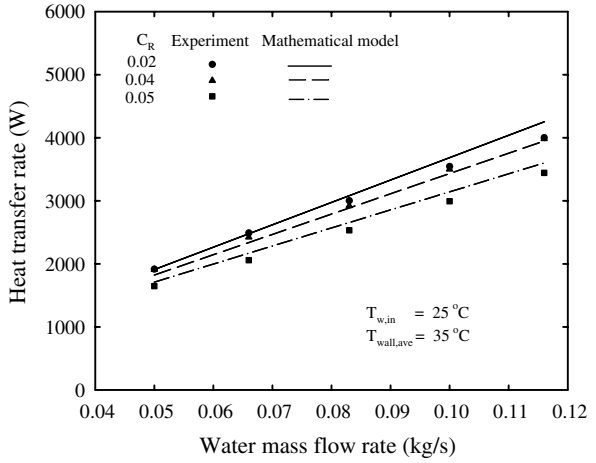

Fig. 7. Variation heat transfer rate with water mass flow rate.

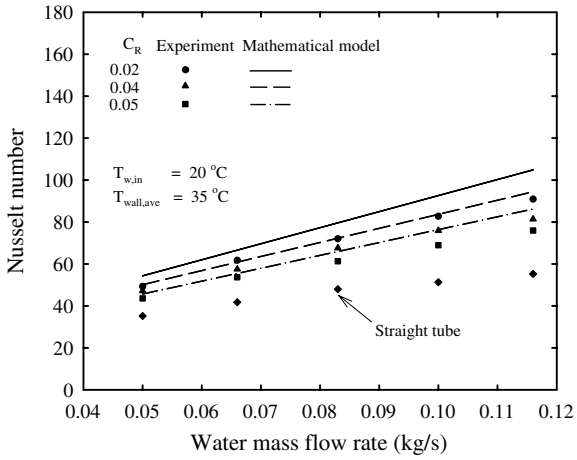

Fig. 8. Variation Nusselt number with water mass flow rate.

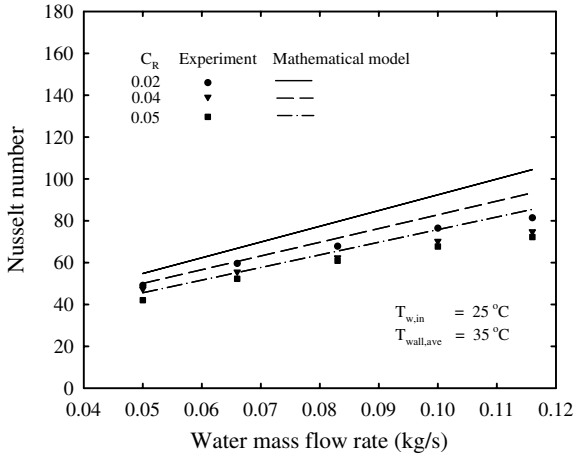

Fig. 9. Variation heat transfer rate with water mass flow rate.

water mass flow rate. This is because the Nusselt number depends directly on the heat removal capacity of the cold water. Due to higher radius curvature, the centrifugal force also increases. Therefore, at a given water mass flow rate, the average Nusselt number for lower curvature ratio are higher than those for higher ones across the range of water mass flow rate.

The present numerical study is validated by comparing with the experimental data. The Nusselt numbers obtained from the numerical study slightly overpredict the measured data. This becomes closer at a lower water mass flow rate. Fig. 8 also shows the comparison the Nusselt number obtained from the spirally coiled tube with those from the straight tube. It is found that the Nusselt numbers obtained from the spirally coiled tube are 1.49 times higher than those from the straight tube. This is because the centrifugal force has significant effect on the secondary flow and this flow depends on the curvature ratio of the tube. This secondary flow has significant effect on the mixing of fluid flow.

Fig. 10 shows the variation of pressure drop per unit length with water mass flow rate. It can be clearly seen that

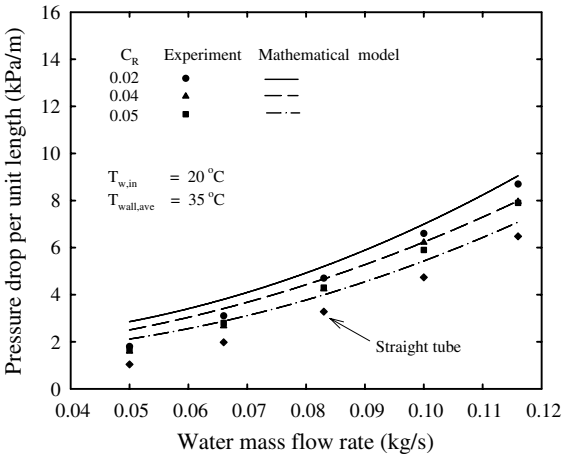

Fig. 10. Variation pressure drop per unit length with water mass flow rate.

the pressure drop tends to increase as water mass flow rate. Across the whole range of water mass flow rate, the average between the measured data is 5.80%. Reasonable agreement is obtained from the comparison between the experimental data and the predicted results. Due to the velocity in radius direction which caused by the centrifugal force, the pressure drop per unit length obtained from higher curvature ratio is lower than that from lower ones. In addition, due to the centrifugal force, the measured pressure drops obtained from the spirally coiled tube are 1.50 times higher than those from the straight tube.

6. Conclusion

New experimental data of the convective heat transfer in the spirally coiled tube under constant wall temperature are presented. The numerical computations reveal the developments and distributions of heat transfer and flow fields in the spirally coiled tube. There is reasonable agreement between the numerical results and the present experimental data. In addition, the heat transfer and pressure drop obtained from the spirally coiled tube are compared with those from the straight tube. The secondary flow caused by the centrifugal force has significant effect on the developments and distributions temperature and flow in the spirally coiled tube. Due to the centrifugal force, the Nusselt number and pressure drop obtained from the spirally coiled tube are 1.49, 1.50 times higher than those from the straight tube, respectively.

Acknowledgement

The authors would like to express their appreciation to the Srinakharinwirot University (SWU) for providing financial support for this study. The authors also wish to acknowledge Asst. Prof. Dr. Wanwilai graipetch for computer software, Mr. Bovon Maneejirasonton, Mr. Kajornpot Chamarat, and Miss Jantra Kampo for their assistance in some of the experimental work.

References

[1] P. Naphon, S. Wongwises, A critical review of the heat transfer and flow characteristics in the curved pipes, Renew. Sustainable Energy Rev. 10 (2006) 463–490.

[2] D.G. Prabhanjan, T.J. Rennie, G.S.V. Raghavan, Natural convection heat transfer from helical coiled tubes, Int. J. Therm. Sci. 43 (2004) 359–365.

[3] T.K. Palazoglu, K.P. Sandeep, Effect of tube curvature ratio on the residence time distribution of multiple particles in helical tubes, Lebensm.-Wiss. u.-Technol. 37 (2004) 387–393.

[4] L.C. Ceresa, J. Delatorre, B.G. Silva, V.R. Gueza, C.P. McKay, Atmospheric moisture collection from a continuous air flow through a refrigerated coil tube, Atmos. Res. 71 (2004) 127–137.

[5] T.H. Ko, K. Ting, Entropy generation and thermodynamic optimization of fully developed laminar convection in a helical coil, Int. Commun. Heat Mass Transfer 32 (2005) 214–223.

[6] T.H. Ko, K. Ting, Optimal Reynolds number for the fully developed laminar forced convection in a helical coiled tube, Energy 31 (12) (2006) 2142–2152.

[7] T.H. Ko, Thermodynamic analysis of optimal curvature ratio for fully developed laminar forced convection in a helical coiled tube with uniform heat flux, Int. J. Therm. Sci. 45 (2006) 729–737.

[8] T.H. Ko, Thermodynamic analysis of optimal mass flow rate for fully developed laminar forced convection in a helical coiled tube based on minimal entropy generation principle, Energy Conversion and Management xx (2006) xxx.

[9] Y. Murai, S. Yoshikawa, S. Toda, Structure of air–water two-phase flow in helically coiled tubes, Nuclear Eng. Des. 236 (2006) 94–106.

[10] A. Cioncolini, L. Santini, An experimental investigation regarding the laminar to turbulent flow transition in helically coiled pipes, Exp. Ther. Fluid Sci. 30 (2006) 367–380.

[11] V. Kumar, M. Aggarwal, K.D.P. Nigam, Mixing in curved tubes, Chemical Engineering Science 61 (2006) 5442–5453.

[12] J.C. Ho, N.E. Wijeysundera, S. Rajasekar, T.T. Chandratilleke, Performance of a compact spiral coil heat exchange, Heat Recovery System nas CHP 15 (1995) 457–468.

[13] J.C. Ho, N.E. Wijeysundera, S. Rajasekar, An unmixed-air flow model of a spiral cooling dehumidifying heat transfer, Applied Thermal Engineering 19 (1999) 865–883.

[14] A. Nakayama, N. Kokubo, T. Ishida, F. Kuwahara, Conjugate numerical model for cooling a fluid flowing through a spiral coil immersed in a chilled water container, Numer. Heat Transfer: Part A 17 (2000) 155–165.

[15] P. Naphon, S. Wongwises, An experimental study on the in-tube heat transfer coefficients in a spiral-coil heat exchanger, Int. Commun. Heat Mass Transfer 29 (2002) 797–809.

[16] P. Naphon, S. Wongwises, A study of the heat transfer characteristics of a compact spiral coil heat exchanger under wet-surface conditions, Exp. Therm. Fluid Sci. 29 (2005) 511–521.

[17] P.H. Oosthuizen, D. Nayler, An Introduction to Convective Heat Transfer Analysis, Mc-Graw-Hill, 1999.

[18] B.E. Launder, D.B. Spalding, Mathematical Models of Turbulence, Academic Press, 1973.

[19] H.K. Versteeg, W. Malalasekera, Computational Fluid Dynamics, Longman Group, 1995.

[20] J.P. Van Doormal, G.D. Raithby, Enhancements of the SIMPLEC method for predicting incompressible fluid flows, Numerical Heat Transfer 7 (1984) 147–163.